Non-Destructive Characterization of UO$_{2+x}$ Nuclear Fuels

Reeju Pokharel,[1]* Donald W. Brown,[1] Bjørn Clausen,[1] Darrin D. Byler,[1] Timothy L. Ickes,[1] Kenneth J. McClellan,[1] Robert M. Suter,[2] and Peter Kenesei[3]

[1]Los Alamos National Laboratory, Los Alamos, NM 87544
[2]Carnegie Mellon University, Pittsburgh PA 15213
[3]Argonne National Lab, 9700 Cass Ave., Lemont, IL 60439

*reeju@lanl.gov

Abstract: This article describes the effect of fabrication conditions on as-sintered microstructures of various stoichiometric ratios of uranium dioxide, UO$_{2+x}$, with the aim of enhancing the understanding of the fabrication process and developing and validating a predictive microstructure-based model for fuel performance. We demonstrate the ability of novel, non-destructive methods such as near-field high-energy X-ray diffraction microscopy (nf-HEDM) and micro-computed tomography (μ-CT) to probe bulk samples of high-Z materials by non-destructively characterizing three samples: UO$_{2.00}$, UO$_{2.11}$, and UO$_{2.16}$, which were sintered at 1450°C for 4 hours. The measured 3D microstructures revealed that grain size and porosity were influenced by deviation from stoichiometry.

Introduction

Nuclear fuels operate under extreme temperature, pressure, and radiation conditions. In such environments, it is important that the fuels maintain their thermal and mechanical properties, exhibit dimensional stability, and maintain integrity of the fuel-cladding system, critical to which is the fission gas transport and release to the fuel rod plenum [1]. Ceramic UO$_2$ is the conventional nuclear fuel used in modern nuclear reactors. Microstructure of ceramic fuels is inherently polycrystalline and typically with ≤ 5% porosity [2], where the length scales of both the grains and pores have heterogeneous spatial distributions within the fuel rod. These heterogeneities can result in anisotropic responses of the fuels when subjected to operating conditions.

One of the microstructural features that has an obvious effect on fuel properties and has been extensively studied is the grain size. It is found that grain size has a major influence on fission gas release and fuel swelling rates [3]. At the interfaces of distinct grains, open channels exist, where the diffusion coefficients of fission products drastically change from that in the bulk of the grain, resulting in increased transport and release rates. Thus, increasing the grain size both increases the diffusion distance from interior-to-boundary and decreases the overall interfacial area, reducing release rates at grain boundaries. This makes fuel microstructure consisting of large grains preferable [3–5].

The microstructure of ceramic nuclear fuel, both fresh and post-irradiation, has traditionally been studied with light and electron microscopy techniques [6, 7, 8]. However, these techniques are inherently destructive, making it impossible to perform evolutionary studies of the microstructure of a specific sample. In contrast, high-energy synchrotron X-rays have the capability to non-destructively probe bulk microstructures [9, 10] and provide information on crystal orientations, elastic strains, phase densities, and their evolution in polycrystalline metals [11–14]. These methods were recently demonstrated on ceramic samples of high-Z materials [15]. Furthermore, complementary pulsed neutron based imaging techniques are being developed that can non-destructively characterize ceramic and metallic nuclear fuel-cladding systems before and after irradiation [16].

In the present work, we probed the three-dimensional (3D) bulk microstructures of three as-sintered UO$_{2+x}$ samples with varying O/U ratios (2+x) using near-field high-energy X-ray diffraction microscopy (nf-HEDM) and micro-computed tomography (μ-CT) techniques, obtaining non-destructive 3D volumetric measurements and spatially resolved orientation and density reconstructions at unprecedented resolution (~s3 μm, 0.1 deg). Oxygen-rich, hyper-stoichiometric UO$_{2+x}$ was expected to sinter faster, resulting in higher-density fuel. In addition, hyper-stoichiometric samples showed higher rate of grain growth for the same sintering conditions. The motivation was to study the effect of oxygen content on sintering microstructure (mainly grain size and porosity) using non-destructive techniques and to demonstrate the kind of information that can be extracted from probing high-Z materials with the intent of providing 3D microstructure data to the modeling community in general, where such data are currently lacking.

Materials and Methods

Sample preparation. For this study, UO$_{2+x}$ fuel pellets, where x is the degree of hyper-stoichiometry, were fabricated from powders with varying stoichiometry. The samples were prepared from an as-received AREVA depleted UO$_2$ powder with an oxygen/metal (O/M) ratio of 2.16. The powder feedstock was milled in a zirconia spex mill jar
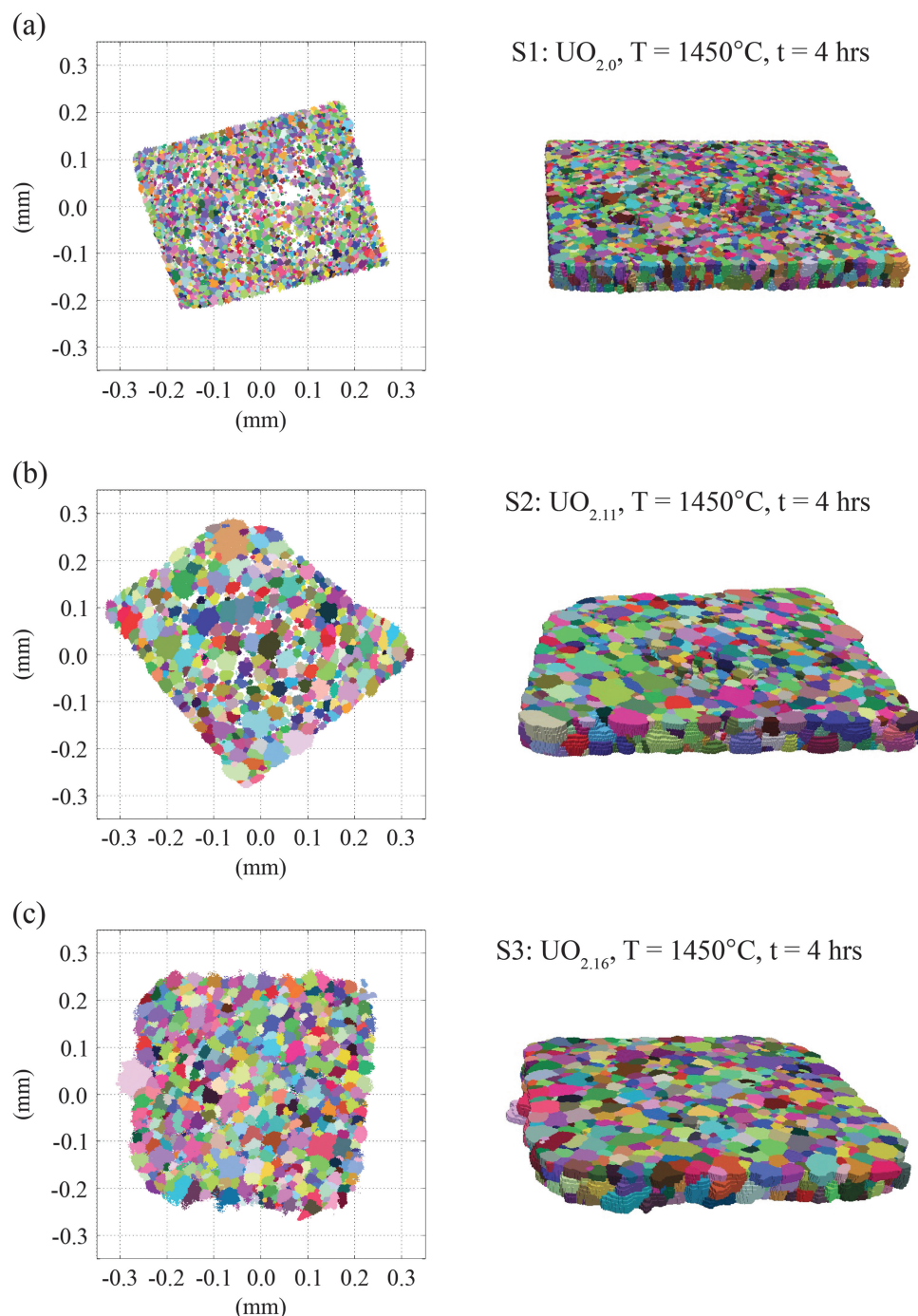
Table 1: Initial state of the bulk as-sintered samples.

Sample	O/U	Bulk density (%)	Porosity (%)	Temperature (°C)	Time (hrs)
S1	2.00	91.43	8.75	1450	4
S2	2.11	96.28	3.72	1450	4
S3	2.16	95.56	4.44	1450	4
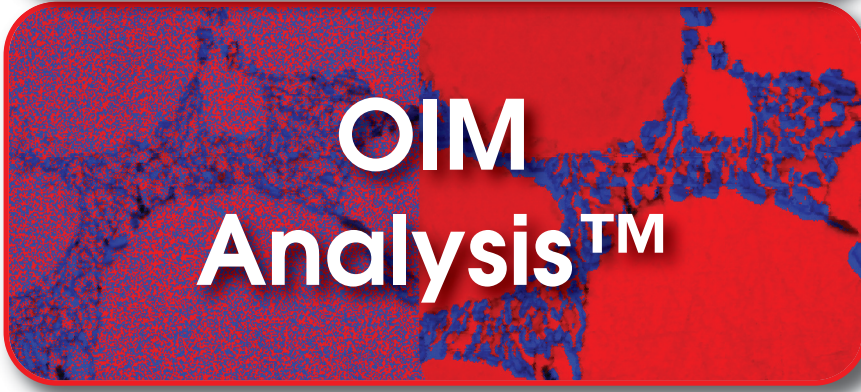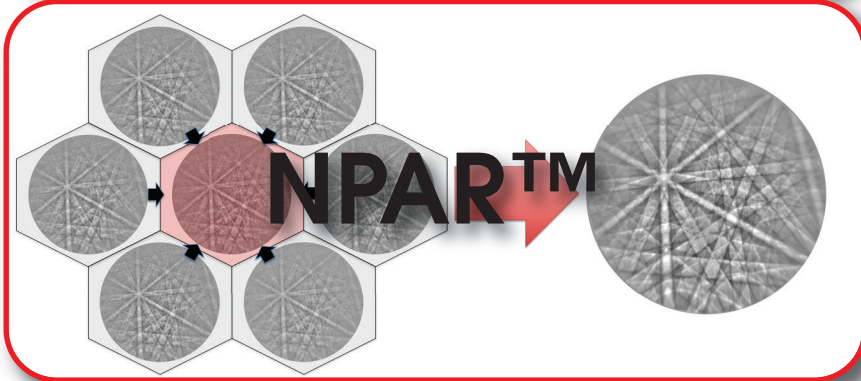
High quality data collection is just the start.....

- **PRIAS™** - an innovative approach for enhancing EBSD sample imaging

- **NPAR™** - a unique way to improve EBSD indexing

- **OIM Analysis™** - a comprehensive toolbox for analysis of EBSD data

- **Hikari EBSD cameras** - combining high speed collection with high precision measurements for results without compromise

AMETEK®
MATERIALS ANALYSIS DIVISION

www.edax.com

EDAX®
Smart Insight

(a)

S1: UO$_{2.0}$, T = 1450°C, t = 4 hrs

(b)

S2: UO$_{2.11}$, T = 1450°C, t = 4 hrs

(c)

S3: UO$_{2.16}$, T = 1450°C, t = 4 hrs

Figure 1: Measurements of 3D microstructures of UO$_2$ pellets with varying oxygen content and sintering temperatures for samples (a) S1, (b) S2, and (c) S3. Left: a single layer in which white areas indicate void locations. Right: entire 3D volumes for S1, S2, and S3. Note that the sample sizes are not all the same.

a specific oxygen partial pressure to obtain the desired O/M ratio for each sample. The witness sample was then reduced in the TGA using the ASTM C1430-07 standard to confirm the final attained O/M of each stoichiometric adjustment to the pellets. Each pellet was then cut using a slow-speed diamond saw and polished using a 30 μm diamond film with water as a lubricant to the final sample dimensions, nominally 0.5 × 0.5 × 1 mm. The final compositions and initial processing conditions of the three samples are summarized in Table 1, including sintering temperature, time, and resulting bulk density.
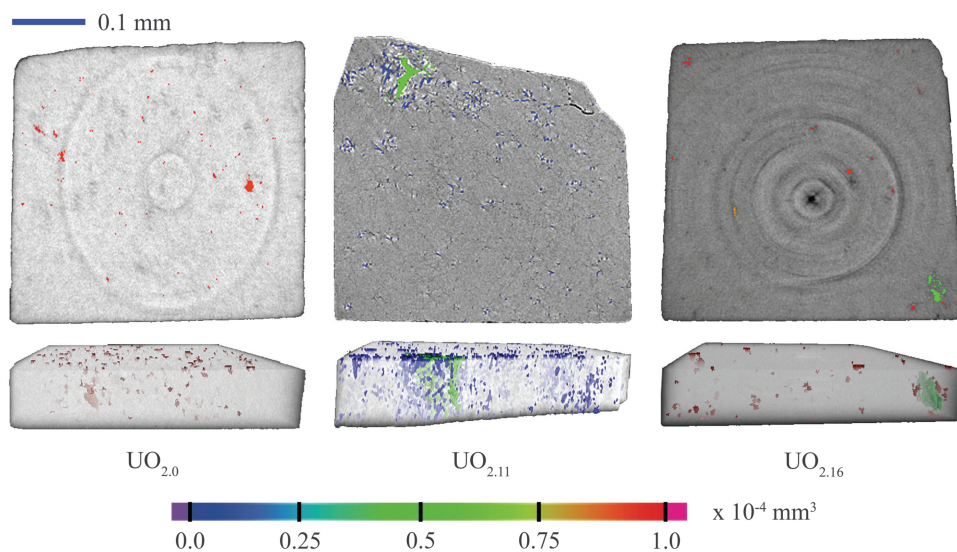
High-energy X-ray techniques. Analysis of the specimens was performed at the advanced photon source (APS) 1-ID-B beam line, where the sample was illuminated with high-energy (85 keV) X-rays. To ensure that data from all of the grains in the illuminated section was captured, the sample was rotated about a vertical axis, perpendicular to the incident beam, and diffraction patterns were collected at 1-degree integration intervals. 3D data were collected by translating the sample in vertical steps of 4 μm, with 2D diffraction data collected for each slice. Tomography data were collected on the near-field detector by removing the focusing optics and increasing the beam height to cover 500 μm in the vertical direction.

The diffraction data obtained from the near-field detector was analyzed using IceNine software [17], which uses the forward model method (FMM) to obtain orientation field maps in both two and three dimensions [10,18]. Simulated diffraction is compared with the measured diffraction pattern; the ratio of overlap between simulated and measured diffraction is given by the confidence index of the fitted microstructure. Since the measurements were performed in a layer-by-layer basis, the fitted layers were stacked in the vertical direction to obtain a 3D volume. Tomographic reconstruction to obtain the density maps was performed using RECON software, developed at LANL [19].

Results

3D microstructure characterization. Initial states of the samples were characterized using nf-HEDM and μ-CT

with one .375 mm zirconia ball for 15 minutes followed by sieving. The powder was then pressed at 40 MPa in a 5.7 mm dual-action custom punch and die set. The pellet was sintered in a gettered argon atmosphere at 1450°C for 4 hrs. The sintered density of the pellet was approximately 10.19 g/cc (~93% theoretical density), and a calculated O/M of 2.04 was based on mass losses during sintering. Then a witness sample and the fuel pellet were put in a thermogravimetric analyzer (TGA) connected to a gas mixing system to achieve

UO$_{2.0}$ UO$_{2.11}$ UO$_{2.16}$

0.0	0.25	0.5	0.75	1.0	x 10⁻⁴ mm³

Figure 2: Volumetric density maps of UO$_{2+x}$ fuel pellets showing that porosity decreased as the stoichiometric ratio changed from UO$_{2.0}$ to UO$_{2.16}$.

value, except that it ignores pores that are smaller than 3 μm, which can add up to being a significant amount. Regardless, it provides a quantitative comparison relative to individual samples.

Table 2 gives the approximate porosity present in each of the three measured samples, which are in close accord with the estimated bulk density. For S3, the estimated porosity deviates largely from that of the bulk measurements. This could be because of homogeneously distributed smaller pores, which are below the resolution limit of HEDM measurements. This assumption is further justified by the tomography map, which shows smaller pore sizes randomly distributed throughout the S3 sample. On the other hand, S2, which has smaller porosity compared to S3, shows good agreement with bulk measurements. This could be because of the presence of large voids in the sample, some of which can be seen on the tomographic images that have slightly higher resolution than the nf-HEDM maps.

Grain-size distribution. Individual grains were segmented from the nf-HEDM orientation map, and grain size was given by sphere-equivalent diameter. Figure 3 shows a quantitative comparison of grain size distributions extracted from the three measured microstructures. Individual colored markers represent the binned grain sizes for each distribution, and the solid curve is a Gaussian distribution fit to the experimental data. The statistical parameters obtained from the fit are summarized in Table 3. First-order moments were calculated from each fit shown in Figure 3.

Specimens S1, S2, and S3 exhibit significant differences in grain-size distributions, despite being created under the same sintering conditions. Assuming similar volume measurements, the stoichiometric sample has more than three times as many grains as either of the two hyper-stoichiometric samples. The total grain numbers for S1, S2, and S3 were 7798, 2164, and 1828, with average grain size of 6.6 μm, 12.7 μm, and 15.4 μm, respectively. Average grain size increased as a function of x, and with increasing x the distributions seemed to have broadened as suggested by the standard deviations 4.6 μm, 7.1 μm, and 7.9 μm for S1, S2, and S3, respectively.
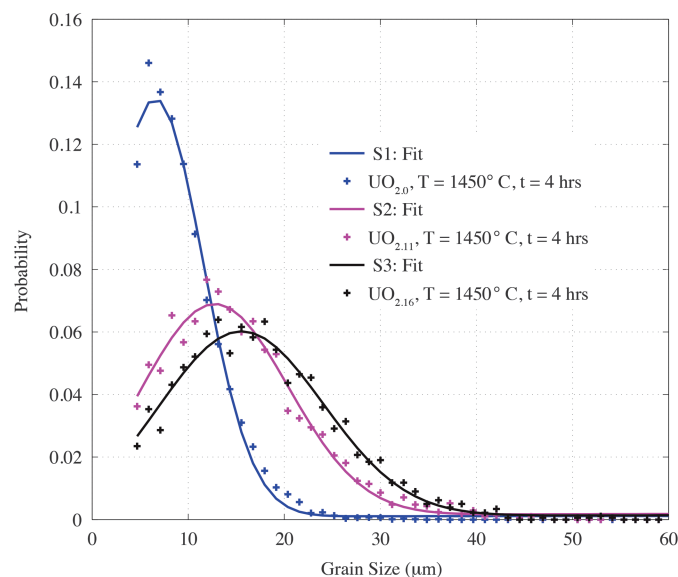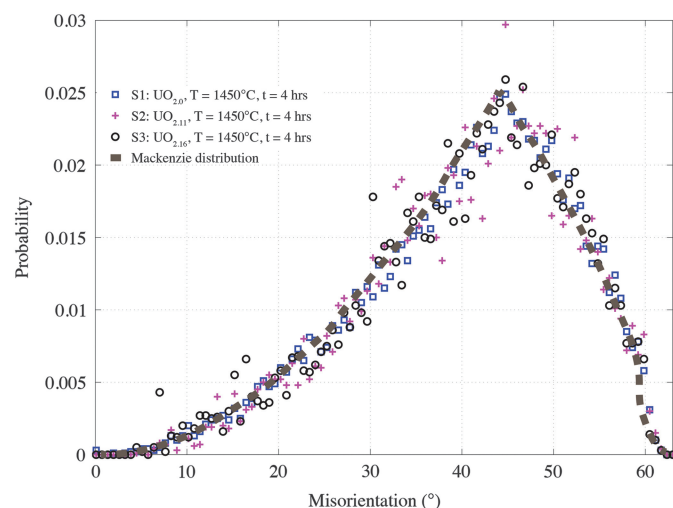
Misorientation distribution. From the measured microstructures, a preference for a specific boundary type after sintering is quantified by calculating grain-boundary

techniques. Crystallographic orientation field information was obtained from the nf-HEDM method, where for each sample, 10 layers were measured approximately spanning a 0.35 × 0.35 × 0.04 mm³ volume with an in-plane resolution of ~3.0 μm and an out of plane resolution of 4 μm. The results are shown in Figure 1, where colors correspond to specific crystal orientations and clusters of similar orientations represent a single grain. The sintering process resulted in UO$_{2+x}$ pellets that were not 100% dense, as noted in Table 1, which can be seen as white spaces in the 2D orientation field maps. Visually, the orientation maps show large variability in grain sizes between the stoichiometric and hyper-stoichiometric microstructures.

The μ-CT measurements were performed on all three samples to obtain density maps. Figure 2 illustrates both single slice and volumetric density maps, which further confirms the presence of interior pores. The color bar represents pore volume. Isolated pores as well as clusters of large voids are obvious from these density maps, indicating heterogeneous porosity distribution. However, the limited quality of the absorption data restricted us from extracting reliable statistics from the reconstructed 3D volumes.

For this study, relative porosity statistics were estimated using the microstructure maps shown in Figure 1. Elements that were not indexed by the FMM software were regarded as pores. Note that limitations in the diffraction data can result in counting voxels belonging to either grain boundaries or small grains as pores. Therefore, the porosity content estimated from orientation maps would inherently be larger than the actual

Table 2: Estimated porosity from measured microstructures, where a voxel below 0.25 confidence index is considered as unindexed.

State	Material point (× 10⁴ voxel)	Unindexed (× 10⁴ voxel)	Estimated porosity (%)	Bulk porosity (%)
S1	66.2	6.4	8.9	8.75
S2	88.0	3.3	3.6	3.72
S3	103.4	0.43	0.41	4.44

Table 3: Statistics from grain-size distributions. Note the error corresponds to the difference between the measured and the fitted distributions.

State	Avg (μm)	SD (μm)	Max (μm)	Error (%)	Number of grains
S1	6.6	4.6	36.8	2.3	7798
S2	12.7	7.1	62.9	2.1	2164
S3	15.4	7.9	55.3	2.0	1828

Figure 3: Probability distributions of grain size for the three UO_{2+x} samples where solid line indicates a fit to each measured distribution.

Figure 4: Grain-boundary misorientation distribution for the $UO2_{+x}$ samples. The distribution of misorientation angle is random, closely resembling a Mackenzie curve.

misorientation between two adjacent grain boundary voxels. The grain-boundary misorientation distributions are shown in Figure 4 for the three measured samples. Besides a small perturbation in the form of random noise, in general all of the distributions resemble a Mackenzie distribution [20], indicating random texture or no preference for any particular boundary orientations at this stage.

Discussion

Current microstructure data infer that average grain size increases with x in UO_{2+x}, provided the sintering conditions, density, and porosity are similar. Normally, the grain growth in stoichiometric UO_2 is expected to be slower than in specimens with $x > 0$ [21] because of the requirement of having to overcome a higher energy barrier for the $x = 0$ specimen [22]. The grain-size distribution in Figure 3 shows a clear trend of increasing average grain size with increasing x. The observed trend suggests that increasing oxygen content contributes to accelerating thermally activated densification, leading to decreased porosity in hyper-stoichiometric samples, as seen in Table 1. For the as-sintered samples, the grain-boundary misorientation distribution was found to be random. Note that the pressing direction during sintering might have been expected to impart some anisotropy at some point, but that was not observed.

Although absorption data were collected for all three samples, because of the novelty of the samples and the measurements, apparently the optimal experimental setup was not realized, resulting in measurement inconsistencies (such as variable sample-to-detector distances) during data collection for the three samples. Thus, quantitative information on pore sizes could not be extracted for these samples. Therefore, nf-HEDM orientation maps were used for porosity quantification, but this method is significantly limited by its spatial resolution. As a result, a large discrepancy between the estimated and bulk porosity was observed, especially for sample S3. The limited spatial resolution of nf-HEDM maps could have missed all pores that were smaller than ~3 μm. In addition to that there is a higher chance that the grain-boundary voxels could have been unindexed and counted toward porosity volume. However, future measurements could be improved by determining a fixed sample-to-detector distance that is suitable for all samples, improving the absorption contrast by collecting transmission data with higher angular resolution, increasing integration time, and reducing the sample-to-detector distance.

Conclusion

In this work, we have demonstrated the viability of the HEDM techniques on a high-Z material. Non-destructive techniques enabled both spatially resolved orientation and density measurements of the UO_{2+x} samples. We observed increased sintering kinetics for hyper-stoichiometric samples. The measurements shown here push the limits of both HEDM and μ-CT techniques because we have measured grains and pores below 5 μm for a high-Z material. Work is in progress to develop next-generation instrumentation in order to perform *in-situ* experiments mimicking

operating conditions such as high temperature and radiation environment.

References

[1] JA Turnbull and MO Tucker, *Philos Mag* 30(1) (1974) 47–63.
[2] FA Nichols, *J App Phys* 37(13) (1966) 4599–4602.
[3] OV Khoruzhii et al., *J Nucl Mater* 265(1) (1999) 112–6.
[4] JA Turnbull, *J Nucl Mater* 50(1) (1974) 62–8.
[5] FR Campbell et al., *Transient Fission Gas Release Rates within UO$_2$ Fuel Elements Following Power Increases.* Atomic Energy of Canada Ltd., Chalk River, Ontario, 1974.
[6] X-Y Liu et al., *J Mater Sci* 47(21) (2012) 7367–84.
[7] PV Nerikar et al., *J Am Ceram Soc* 94(6) (2011) 1893–900.
[8] K Rudman et al., *Nucl Technol* 182(2) (2013) 145–54.
[9] HF Poulsen, *Three-Dimensional X-Ray Diffraction Microscopy: Mapping Polycrystals and Their Dynamics* volume 205##Springer Science & Business Media, New York, 2004.
[10] RM Suter et al., *Rev Sci Instrum* 77(12) (2006) 123905.
[11] R Pokharel et al., *Int J Plasticity* 67 (2015) 217–34.
[12] JC Schuren et al., *Curr Opin Solid St M* 19(4) (2015) 235–44.
[13] A Cerrone et al., *Modell Simul Mater Sc* 23(3) (2015) 035006.
[14] CM Hefferan et al., *Acta Materialia* 60(10) (2012) 4311–8.
[15] DW Brown et al., *Mater Sci Forum* 777 (2014) 112–7.
[16] SC Vogel et al., *Non-destructive Pre-irradiation Assessment of UN / U-Si "LANL1 ATF Formulation.* Los Alamos National Laboratory (LANL), Lemont, IL, 2016.
[17] SF Li. Orientation Reconstruction for Synchrotron X-ray Data," https://github.com/frankieli/icenine, 2013.
[18] SF Li and RM Suter, *J Appl Crystallogr* 46(2) (2013) 512–24.
[19] J Hunter et al., *Overview of tomography developments at LANL.* Los Alamos National Laboratory (LANL), Lemont, IL, 2011.
[20] JK Mackenzie, *Acta Metall* 12(2) (1964) 223–5.
[21] MJ Bannister and WJ Buykx, *J Nucl Mater* 64(1–2) (1977) 57–65.
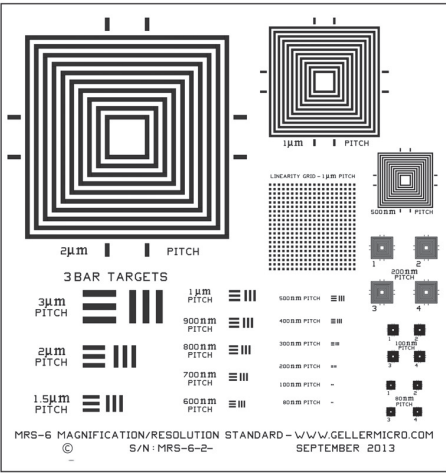[22] I Amato et al., *J Am Ceram Soc* 46(8) (1963) 407–7.

Mт